Available online at www.sciencedirect.com

ScienceDirect

Physics Procedia 83 (2016) 909 – 917

Physics Procedia

9th International Conference on Photonic Technologies - LANE 2016

A novel processing approach for additive manufacturing of commercial aluminum alloys

Christopher E. Roberts[a,*], David Bourell[a], Trevor Watt[a], Julien Cohen[a]

[a]*The University of Texas at Austin, 204 E. Dean Keeton Street, Austin, Tx 78712, United States of America*

Abstract

Aluminum 6061 is of great commercial interest due to its ubiquitous use in manufacturing, advantageous mechanical properties, and its successful certification in aerospace applications. However, as an off-eutectic with accompanying large freezing range, attempts to process the material by additive manufacturing have resulted in part cracking and diminished mechanical properties. A unique approach using mixed powders is presented to process this historically difficult-to-process material. Expansion of this combined-powder approach to other materials systems not typically compatible with additive manufacturing is possible. Dense parts without solidification cracking have been produced by the SLM process, as verified using SEM and EDS. An overview of this approach is presented along with test results using an Al-Si mixture.

Peer-review under responsibility of the Bayerisches Laserzentrum GmbH

Keywords: SLM; selective laser melting; aluminum; AA6061; elemental mixture

1. Introduction

Aluminum alloy 6061, composed of aluminum with approximately 1% magnesium, 0.6% silicon and trace amounts of copper and chromium, is widely used throughout industry including aerospace and marine sectors due to its acceptable weldability and excellent corrosion resistance as discussed in Al-303 of ASM (2002). Since this alloy has been approved for safety critical applications, commercial interest is high in developing an approach to additive manufacturing (AM) the alloy.

* Corresponding author. Tel.: +1-256-5089713 .
E-mail address: cer0009@utexas.edu

Peer-review under responsibility of the Bayerisches Laserzentrum GmbH
doi:10.1016/j.phpro.2016.08.095

Currently AlSi10Mg, closely related to the aluminum casting grade A360, is the most popular alloy for selective laser melting (SLM). Durbin (2005) notes that the aluminum silicon system exhibits high fluidity and low shrinkage leading to its use in casting, brazing and welding applications. When present in significant quantities, as in AlSi10Mg, silicon decreases the melting range of the of the alloy and increases hot tearing resistance without introducing brittleness as discussed by Davis et al. (1993). By decreasing the melt range, dendritic cooling and shrinkage in the mushy zone is reduced prior to full solidification, leading to decreased void generation and hot tearing.

However unlike AlSi10Mg, AA6061 belongs to the wrought class of aluminum alloys. Low silicon content and large shrinkage inhibit many of the advantageous properties associated with the aluminum silicon casting series. Data provided by ASM (2002) Al-303 and Al-308 show that hypoeutectic AA6061 possesses a freezing range of approximately 70 K verses 20 K for A360, resulting in increased hot tearing especially during the highly non-equilibrium processes observed during SLM. Furthermore, the rapid formation of an oxide layer, high solubility limit of hydrogen and high thermal conductivity and thermal expansion coefficient of aluminum present several technical challenges when processing these alloys. Thus, much of the research into processing off-eutectic aluminum alloys and in particular AA6061, has shown unacceptable levels of cracking, highly anisotropic microstructures, and porosity as discussed by Benjamin et al. (2014) and Louvis et al. (2011). As stated by Bourell et al. (2009) in the "Roadmap for Additive Manufacturing", the primary challenge for additive manufacturing with regards to materials is developing consistent quality parts in a wider variety of materials. Therefore, it is of great research and industrial interest to determine novel approaches to processing off-eutectic alloys not suitable to traditional AM approaches.

The primary feedstock for laser based additive manufacturing remains pre-alloyed powder or wire. Others including Clayton (2013), D. D. Gu et al. (2012), and Schwendner et al. (2001) have researched the use of elemental powder mixtures in both traditional powder metallurgy and in additive manufacturing. However, these studies have focused on reducing processing cost or manufacturing functionally graded components. Vora et al. (2015) presented *in situ* alloying of near-eutectic AlSi12 as a method to reduce residual stress in anchorless SLM, by utilizing the melting point depression of eutectic alloys to form a "super cooling" like behavior. In spite of this, research has not been done focusing on utilizing elemental mixtures to ease the processing of difficult-to-AM-process materials. Furthermore, success has been limited in AM processing and traditional powder metallurgy of hypoeutectic aluminum alloys as noted by D. D. Gu et al., 2012; Mosher et al., 2011. In contrast, current research into the use of pure metals in SLM has been successful for titanium, copper, gold, and magnesium systems as discussed by Becker and Wissenbach (2009), Chung Ng et al. (2011), D. Gu et al. (2012), D. D. Gu et al. (2012) and Khan and Dickens (2010). The purpose of the present undertaking is to demonstrate an approach to AM processing of metal alloys by processing elemental powders followed by homogenization post-processing.

2. Methodology

To process off-eutectic metals, an elemental mixture of aluminum and silicon powders was utilized to mimic the final composition of AA6061. The use of magnesium or magnesium silicide powder was avoided in this initial analysis due to safety concerns and the significantly reduced effect magnesium has on alloy melt range (10 K at 1.0 wt.% Mg) compared to silicon (70 K at 0.6 wt. % Si). While aluminum alloys do show high solidification crack sensitivity to the addition of copper, the concentration of copper in AA6061 is relatively low. Furthermore, the high cooling rates sassociated with SLM, do not alloy for complete alloying minimizing the impact of copper. Thus, silicon was predicted to have the highest impact on solidification cracking and selected as the first alloying element for study. Due to the relatively high melting point of silicon compared to aluminum, low build chamber temperature, and the short thermal cycle during the laser scan, the silicon is believed to remain in the solid state without long range diffusion into the surrounding aluminum. Thus, the aluminum melts and encapsulates the silicon particles. Post-SLM homogenization treatment would then have the dual advantage of relieving residual stress and dissolving the silicon throughout the aluminum matrix. Since any pure metal melts congruently, the challenges associated with hot tearing due to solidification in the mushy zone is negated. Thereby, the major issue presented by hypoeutectic alloys during AM powder bed processing may be overcome.

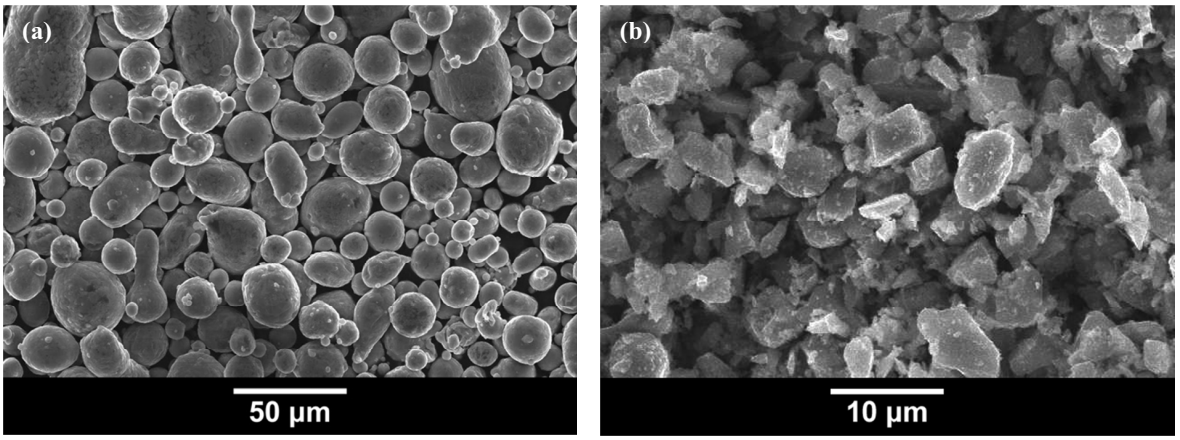

Fig. 1. Secondary electron images of (a) aluminum powder sourced from Valimet showing nearly spherical morphology, and (b) fine silicon powder characterized by faceted surfaces.

To better understand conditions that result in solidification cracks and to determine the effect of processing parameters on crack formation, an initial build was conducted utilizing pre-alloyed AA6061. Subsequently, during the first build stage utilizing an elemental mixture, dissolution of the silicon into the aluminum matrix was of primary concern. To assess the feasibility of this approach, a powder mixture was prepared with 0.6% silicon powder and 99.4% aluminum powder. It was processed using SLM and then post-processed to dissociate the Si phase.

2.1. Feedstock powders

Initial feedstock for the elemental powder study was -325 mesh aluminum and silicon powder. The aluminum feedstock was obtained from Valemet and consisted of highly spherical atomized powder with a minimum purity of

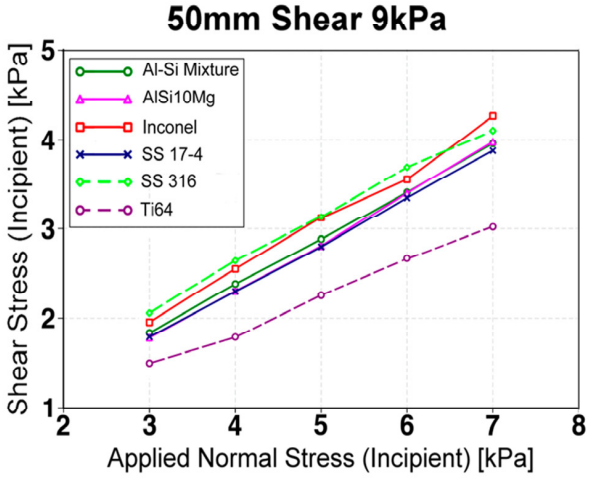

Fig. 2. Shear cell testing results comparing the elemental mixture to commercially available additive manufacturing feedstock.

99.7% as seen in Fig. 1(a). The silicon powder, obtained from Alfa Aesar with a purity of 99.5%, exhibited a highly faceted surface structure which a mean particle size of approximately 4 µm shown in Fig. 1(b). The powders were combined in the weight fraction of 99.4%Al-0.6% Si and then mixed on medium speed for 5 hours utilizing a U.S. Stoneware 802CVM ball mill with no additional media. The particle size distribution (PSD) for the mixed powder

and comparison feedstocks were analyzed using a MicroTrac S3500, with a volumetric-mean particle size of 35.49 μm and a standard deviation of 15.45 μm. Shear cell analysis using a FT-4 Powder Rhometer indicated good comparison to commercially available additive manufacturing powders as shown in Figure 2.

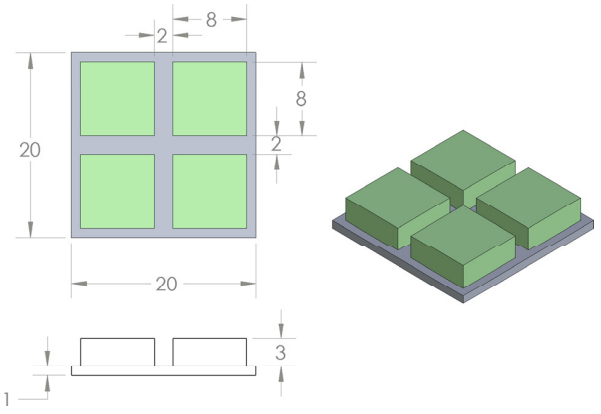

Fig. 3. Sample geometry for AA6061 and Al-Si AM builds. Dimensions are in mm.

Table 1. AM parameter set for the Al-Si Elemental Powder SLM Run.

Sample Number	Beam Power (W)	Scan Speed (mm/s)	Average Energy (J/cm^2)
1	313	750	516
2	370	544	840
3	258	375	848
4	335	375	3157
5	192	75	4107
6	250	75	1459
7	222	187.5	1898
8	288	187.5	645
9	284	544	1155
10	351	375	1051
11	367	375	525
12	319	375	854
13	370	870	516
14	301	435	840

2.2. Materials processing

All samples were processed at Stratasys Direct Manufacturing (SDM), Belton TX USA, using an EOSINT M280 powder bed fusion machine at a build temperature of 35 ^{0}C. The maximum laser power output from the M280 was 370 W. Samples were prepared in test cubes as shown in Figure 3. This square solid geometry 8 mm by 8 mm by 3 mm allows up to four samples to be placed in a standard 31.8 mm diameter metallographic polishing puck. Given this geometry and the parameters used, each sample consists of approximately 75 build layers and between 40-100 scan tracks per layer.

The initial build utilized AA6061 pre-alloyed powder. Since the primary interest of this build was to determine the effects of laser power, scan speed, and scan spacing on the as-built microstructure, a large spread of processing parameters was employed based upon effective energy density and thermal properties of AA6061. Each as-built sample was ranked based upon surface finish, porosity, and crack density. From this data set, a parameter matrix consisting of 14 parameter sets, shown in Table 1, was developed for the build utilizing the elemental mixture of aluminum and silicon. A correction, utilizing data from H.Y. Hunsicker, L.F. Mondolfo, (1990) was made for the increased melting temperature of the pure aluminum (660^{0}C) as compared to the melting temperature of AA6061 (582-652^{0}C) resulting in an increase of the average energy input by 6.1% compared to the AA6061 results. Additional samples were created utilizing expanded parameters based on the optimal AA6061 results.

2.3. Sample preparation

After SLM AM processing, each sample was sectioned on a low speed diamond saw, cleaned with warm water and ethyl alcohol, then placed in a 31.8 mm diameter mount and encapsulated in epoxy. Each sample was ground and polished using an automated rotary polisher in the following sequence: 500 and 1200 grit SiC paper immersed

in water, followed by 9 μm, 3 μm and 1 μm diamond suspension. Selected samples then underwent final polishing utilizing a 0.04 μm colloidal silica solution.

Heat treatment was necessary to promote diffusion of the silicon throughout the aluminum matrix. Solutionizing times were estimated using random walk analysis, resulting in approximately 20 minute diffusion time. To ensure complete dissolution, samples were heat treated in a furnace at 600^0C for approximately 1 hour. To reduce complexity and cost, an inert environment was not utilized as the solutionizing time was small thereby inhibiting long range diffusion of oxygen resulting in only a thin surface oxide layer. Heat treated samples were sectioned and polished using the same procedure described above.

2.4. Analysis

A range of techniques were utilized to analyze the samples. Prior to sectioning and polishing, images were taken of the top surfaces using a JEOL JSM-5610 scanning electron microscope. Each sample was qualitatively ranked on surface roughness and crack density while any apparent porosity was noted. After cross-sectioning and polishing, each sample was imaged using a Nikon Eclipse ME600 optical microscope with bright and dark field imaging to investigate the presence of cracks and internal porosity. SEM imaging was also performed on certain cross-sectioned samples to determine locations of silicon particles and any additional porosity not seen during optical analysis. Energy-dispersive X-ray spectroscopy (EDS) was performed to determine silicon particle spatial distribution and size on both as-built and heat treated samples. Sample areas were scanned for approximately 10 minutes for data gathering.

3. Results and Discussion

3.1. Aluminum 6061 pre-alloyed feedstock

SLM samples of pre-alloyed AA6061 without post-processing showed evidence of severe cracking throughout. Scan spacing was seen to have little effect on final properties; however, as expected, laser power and scan speed were seen to have a great effect on the initial specimen quality. Moderate laser power and scan speed yielded samples with optimal results. Upon metallographic analysis, both average void size and crack density were greatly reduced in the region encompassing approximately 0.75 mm above the support structures, as shown in Fig. 4 (a). Large thermal gradients are believed to have contributed to crack formation. For the first 500 μm of height there is

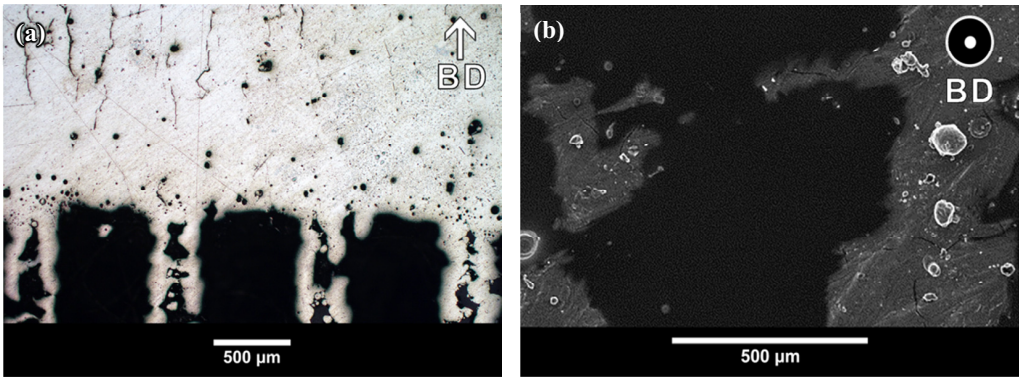

Fig. 4. (a) Optical microscope image of SLM processed AA6061 (343 W, 752 mm/s, 0.13 mm scan spacing) showing evidence of solidification cracking starting approximately 0.75 mm above the support structure. “BD” is the build (+Z) direction; (b) SEM image of dark pools resulting from the segregation of magnesium.

relatively slow cooling due to the poor thermal conductivity of the supporting powder and sparse support structure.

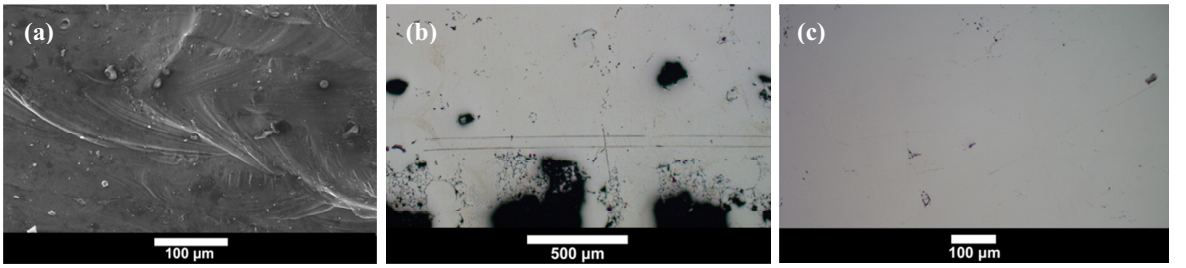

Fig. 5. (a) Surface of elemental Al-Si Specimen 1 (313 W, 750 mm/s), indicating minimal surface cracking or porosity; (b) Sample 12 (319 W, 375 mm/s). Large porous voids are visible along with lines of smaller porosity emanating from the support structure legs; (c) Sample 9 (284 W, 544 mm/s) showed significantly less porosity leading to an acceptable density.

As the solid part height increases, the capacity of the underlying material to extract heat from the melt pool increases, resulting in steeper thermal gradients and larger thermal stresses.

An unexpected finding was dark pools observed on specimen surfaces, shown in Fig. 4 (b). EDS analysis indicated that the pools were associated with an increase in magnesium, carbon, and oxygen content. This is also suggested by the dark shading shown in the secondary electron images, which always have a backscatter electron component where lower atomic number elements (Mg) show up as dark regions compared to the neighboring elements (Al). Segregation of magnesium is likely caused by either the relatively low density of magnesium compared to aluminum resulting in buoyancy-driven flow, segregation-driven flow in the mushy zone due to non-equilibrium solidification, Marangoni flow related phenomena, or some combination of the above. Often these pools were seen near crack formation or on the inside of the crack itself. Furthermore, a decrease in magnesium pool size at high laser power was observed. Laser welding research suggests that high power levels cause the vaporization of magnesium from the melt pool which could result in decreasing pool size.

3.2. Aluminum-silicon elemental mixture

As expected, the as-processed blended Al-Si specimens varied greatly in both surface finish, and fusion defects. While best surface finish was present at high laser power and slow scan speeds, SEM imaging showed the presence of defects especially near the sample number embossed on the surface. Therefore, moderate laser power and medium to high scan speed, similar to that obtained for the best AA6061 specimens, demonstrated optimal properties resulting in two of the samples having relatively low surface defect density at the cost of a slightly rougher surface finish, as shown in Fig. 5a.

Optical analysis of the samples revealed a wide range of porosity as shown in Fig. 5b and Fig. 5c. Many samples showed porosity emanating from the support structures in straight lines, which would then be crossed by a perpendicular line of porosity of similar size as evident in sample 12 shown in Fig. 5b. This phenomenon is believed to be a result of processing conditions and not material dependent porosity related to the parameters in question.

However, all samples showed a significant improvement in crack formation and growth compared to AA6061, as illustrated by Fig. 6. An elemental mixture should behave much like that of the primary component as long all other constituents are relatively dilute. Thus, unlike the pre-alloyed AA6061 feedstock, the elemental mixture will exhibit nearly congruent melting resulting in a freezing point instead of a freezing zone. Therefore, thermal stresses are minimized and hot tearing is avoided. This is evidenced by the lack of solidification cracking seen in the samples produced from the elemental mixture. The morphology of the defects that did appear suggested that the creation of the defect was due to inadequate fusion of the powder which resulted in cracks that followed the outline of the particle boundaries upon cooling versus hot tearing where tendrils partially bridged the crack indicating that the crack formed while the material remained in the mushy state.

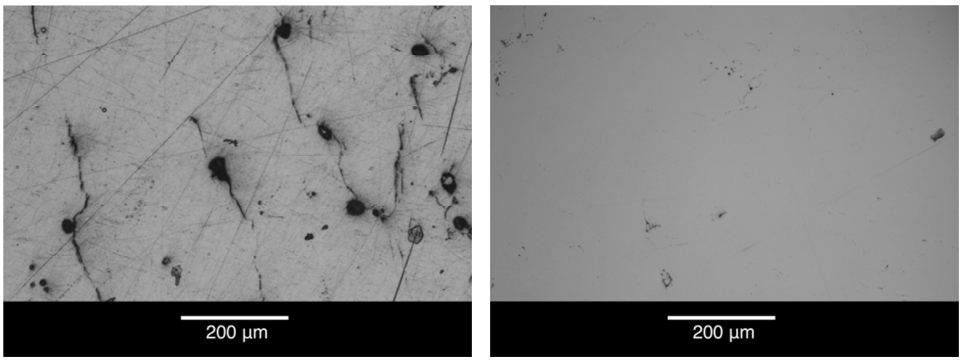

Fig. 6. Comparison of as processed AA6061 (a) and the Al-Si mixture (b).

It is hypothesized that the silicon remains in the solid state throughout the SLM processing of the elemental mixture due to its relatively high melting point and SLM's short thermal cycling times. Therefore, Si particles of similar size and shape as the feedstock should be present in the as-built samples and should be dispersed in a nearly homogeneous distribution. The feedstock consisted of highly faceted silicon particles which had a size distribution of approximately 1-5 µm in diameter with a typical particle possessing a major axis length of approximately 4 µm. To determine the silicon distribution in the as-built samples, EDS was performed on Sample 9. Silicon particles within the image were then magnified and exposed again to determine the size of the particle. As shown in Fig. 7, silicon particles exhibited the predicted morphology, both highly faceted and approximately 4 µm in length along the major axis. This suggests that the silicon particles remained solid within the melt pool during SLM, undergoing minimal dissolution into the surrounding aluminum matrix. Melting remained congruent, and coring was minimized as the melt pool consisted mainly of pure aluminum with trace impurities.

After heat treatment there was a significant derease in the observed number of silicon particles throughout the aluminum matrix, as shown in Fig. 8. However, there remained a few small particles in several images. It is thought that these particles represented the upper range of the particle size distribution of the silicon particles. These particles reduced in size during the post-processing solutionizing anneal but did not completely dissolve due to inadequate time (1hr) at temperature (600 ^{0}C). A longer solutionizing time would further reduce their size and eventually result in complete dissolution. The solutionizing time was kept to a minimum in this study to reduce the oxidation of the surface of the part. By solutionizing the sample in a furnace open to the air, cost and complexity are reduced leading to a more economically viable process.

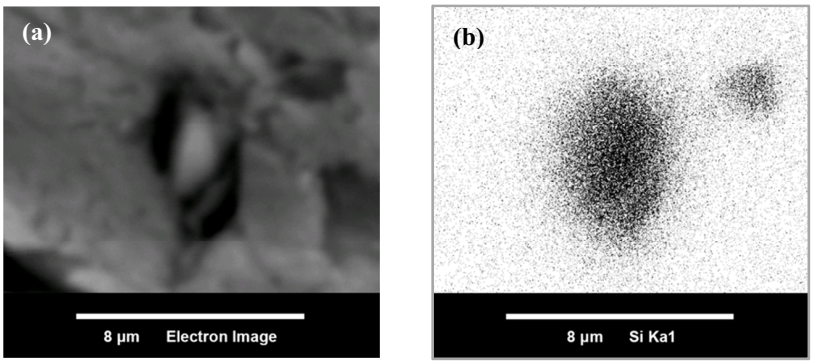

Fig. 7. SEM image (a) and associated EDS Si elemental map (b) illustrating the silicon particle location. The larger of the two silicon particles shown in the image measured 4.53 µm along the major axis. Silicon rich regions appear as dark features.

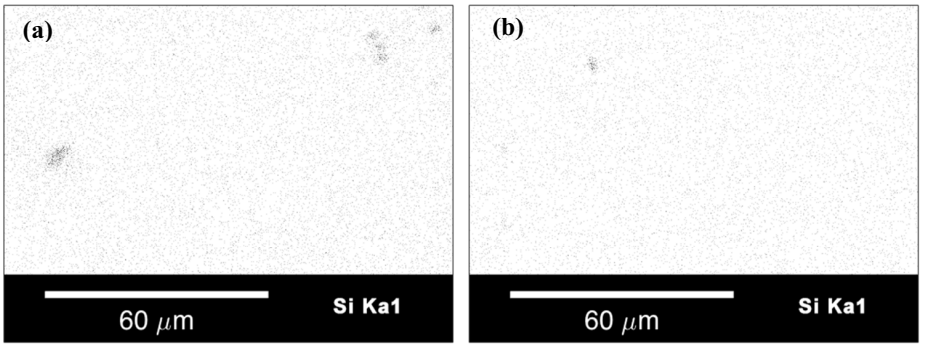

Fig. 8. Comparison of the as built Al-Si elemental mix after SLM. Silicon rich regions appear as dark features. (a) and after post processing (b). It can be seen that both the number and size of the particles have been greatly reduced after heat treatment. However, one particle is still present in the heat treated sample.

4. Conclusion

Elemental mixtures show promise in eliminating solidification cracking in off-eutectic alloys. An aluminum silicon mixture was processed and shown to form an alloy after heat treatment. Optimal processing conditions were shown to occur at moderate laser power and scan speed. However, research into the addition of other alloying elements is needed as well as a better understanding of the resulting microstructure in the as-processed material and the post-heat treated sample.

Acknowledgements

The authors would like to thank Ben Fulcher (Stratasys Direct Manufacturing) for SLM-processing the materials, particle size density analysis, and shear cell testing.

References

ASM, 2002. Alloy Digest, Alloy Digest. ASM International, Orange, N.J.

Becker, D., Wissenbach, K., 2009. Additive Manufacturing of Copper Components with Selective Laser Melting, Fraunhofer ILT Annual Report. Aachen Germany.

Benjamin, F.A., Leigh, D.K., Watt, T.J., 2014. Comparison of AlSi10Mg and Al 6061 Processed Through DMLS. In: SFF Symposium Proceedings. Austin, 404-419.

Bourell, D.L., Leu, M.C., Rosen, D.W., 2009. Roadmap for Additive Manufacturing: Identifying the Future of Freeform Processing. University of Texas, Lab for Freeform Fabrication.

Chung Ng, C., Savalani, M., Chung Man, H., 2011. Fabrication of magnesium using selective laser melting technique. Rapid Prototyp. J. 17, 479–490.

Clayton, R.M., 2013. The use of elemental powder mixes in laser-based additive manufacturing. Masters Thesis. Missouri University of Science and Technology.

Davis, J.R., Associates, J.R.D.&, Committee, A.S.M.I.H., 1993. Aluminum and aluminum alloys, ASM specialty handbook. ASM International.

Durbin, T.L., 2005. Modeling Dissolution in Aluminum Alloys. Georgia Institute of Technnology.

Gu, D., Hagedorn, Y.-C., Meiners, W., Meng, G., Batista, R.J.S., Wissenbach, K., Poprawe, R., 2012. Densification behavior, microstructure evolution, and wear performance of selective laser melting processed commercially pure titanium. Acta Mater. 60, 3849–3860.

Gu, D.D., Meiners, W., Wissenbach, K., Poprawe, R., 2012. Laser additive manufacturing of metallic components: materials, processes and mechanisms. Int. Mater. Rev. 57, 133–164.

H.Y. Hunsicker, L.F. Mondolfo, P.A.T., 1990. Properties of Pure Metals, Properties and Selection: Nonferrous Alloys and Special-Purpose Materials. ASM Handbook Vol 2.

Khan, M., Dickens, P., 2010. Selective Laser Melting (SLM) of pure gold. Gold Bull. 43, 114–121.

Louvis, E., Fox, P., Sutcliffe, C.J., 2011. Selective laser melting of aluminium components. J. Mater. Process. Technol. 211, 275–284.

Mosher, W.G., Kipouros, G.J., Caley, W.F., Donaldson, I.W., Bishop, D.P., 2011. On development of hypoeutectic aluminium–silicon powder metallurgy alloy. Powder Metall. 54, 432–439.

Schwendner, K.I., Banerjee, R., Collins, P.C., Brice, C.A., Fraser, H.L., 2001. Direct laser deposition of alloys from elemental powder blends. Scr. Mater. 45, 1123–1129.

Vora, P., Mumtaz, K., Todd, I., Hopkinson, N., 2015. AlSi12 In-Situ Alloy Formation and Residual Stress Reduction using Anchorless Selective Laser Melting. Addit. Manuf. 7, 12–19.